

Angle-resolved magnetoresistance in the strongly anisotropic quantum magnet TmB_4

Július Bačkaitis^{1,2}, Slavomír Gabáni^{1,*}, Gabriel Pristáš¹, Matúš Orendáč¹, Emil Gažo¹, Kirill Krasnikov³, Nikolay Sluchanko³, Konrad Siemensmeyer⁴, Natalya Shitsevalova⁵ and Karol Flachbart¹

¹*Institute of Experimental Physics, Slovak Academy of Sciences, Watsonova 47, 040 01 Košice, Slovakia*

²*Faculty of Electrical Engineering and Informatics, Technical University, Letná 9, 04200 Košice, Slovakia*

³*Prokhorov General Physics Institute, Russian Academy of Sciences, Vavilov 38, Moscow 119991, Russia*

⁴*Helmholtz-Zentrum Berlin, Hahn-Meitner Platz 1, 14109 Berlin, Germany*

⁵*Institute for Problems of Materials Science, National Academy of Sciences of Ukraine, Krzhizhanovskyy 3, 036 80 Kiev, Ukraine*



(Received 22 July 2022; revised 10 March 2023; accepted 15 March 2023; published 4 April 2023)

Precise angle-resolved magnetoresistance (ARMR) measurements in various magnetic fields enabled us to create illustrative distributions of $\Delta\rho/\rho(\varphi, H)$ in TmB_4 , where φ is the angle between the sample c axis and applied magnetic field H . These distributions reveal the charge transport anisotropy in this strongly Ising anisotropic quantum antiferromagnet with a geometrically frustrated Shastry-Sutherland lattice exhibiting fractional magnetization plateaus. While in the paramagnetic region $\Delta\rho/\rho(\varphi, H)$ reaches its maxima for $H \perp c$, below the Néel temperature $T_N = 11.7$ K the situation is different. Here the main MR features appear for $H \parallel c$, i.e., along the easy axis of magnetic anisotropy, and correspond to magnetic phases and phase transitions between them. It is interesting that all the above features (maxima) related with the scattering of conduction electrons on spin magnetic structure are related with fractional magnetization plateaus. With increasing φ MR anomalies shift to higher fields. Above the field of magnetic saturation, moreover, significant MR maxima have been observed at certain angles which correspond to specific directions in the crystal lattice, pointing to field directions in which the scattering of conduction electrons on the magnetic structure is the highest. Thus, ARMR appears to be a sensitive experimental tool reflecting the angular dependence of the interplay between charge carriers and magnetic structure as a function of temperature and applied magnetic field.

DOI: [10.1103/PhysRevB.107.144403](https://doi.org/10.1103/PhysRevB.107.144403)

I. INTRODUCTION

Properties of quantum spins with antiferromagnetic (AFM) coupling on frustrated lattices have attracted widespread interest in recent years due to the discovery of a variety of new quantum ground states such as, e.g., spin ice [1], quantum spin-liquid-like states [2], and fractional magnetization plateaus on the Shastry-Sutherland lattice (SSL) [3], among them the insulating $\text{SrCu}_2(\text{BO}_3)_2$ [4] as well as the family of metallic rare earth (RE) tetraborides, REB_4 [5–17]. In the case of RE tetraborides, even if they crystallize in the same frustrated magnetic lattice as $\text{SrCu}_2(\text{BO}_3)_2$, the phase diagrams of REB_4 magnetic compounds show different properties. In insulating $\text{SrCu}_2(\text{BO}_3)_2$ the exchange interaction is of the Heisenberg type, while on the other hand in metallic REB_4 magnets the AFM exchange interaction between their magnetic moments is of long-range Ruderman-Kittel-Kasuya-Yosida (RKKY) type mediated by conduction electrons. In such systems also the transport properties can be strongly influenced by the magnetic structure. This interplay between charge carriers and magnetism therefore allows the use of transport experiments as an indirect probe of the magnetic anisotropy that is present both in the paramagnetic and magnetically ordered phases in these model systems.

Thulium tetraboride TmB_4 probably is the most investigated compound of this series. It orders antiferromagnetically at $T_N = 11.7$ K and has attracted attention for its rich magnetic phase diagram which is strongly biased by crystal field effects at Tm^{3+} ion sites that lift the degeneracy of the $J = 6$ multiplet and lead to a $M_J = \pm 6$ ground state doublet [5,18–22]. TmB_4 thus exhibits strong Ising anisotropy where the magnetic field of saturation along the c axis is at least ten times smaller than in the perpendicular a - b plane. The most distinctive features of magnetization M along the c axis are various fractional magnetization plateaus which depend on applied field H . A wide main plateau with $M/M_{\text{SAT}} = 1/2$ arises in fields between about 17.5 and 36 kOe, and narrow fractional plateaus with $M/M_{\text{SAT}} = 1/11, 1/9, 1/8,$ and $1/7$ in fields between about 14 and 17.5 kOe (see, e.g., [5,23]). At low fields, below about 14 kOe, the antiferromagnetic ground state phase consists of an AFM arrangement of thulium ion dimers, where the dimer spins are ferromagnetic (see Fig. 1). Very recent results concerning the properties of fractional plateaus based mainly on magnetization and heat capacity measurements can be found in [24–26].

Nevertheless, in electrically conducting TmB_4 , as mentioned above, also conducting electrons can provide additional information about various magnetic states. Such information, based on resistivity, magnetoresistance (MR), and Hall effect measurements, were recently obtained in [22,27,28]. They show that electronic transport as a function of temperature and

*gabani@saske.sk

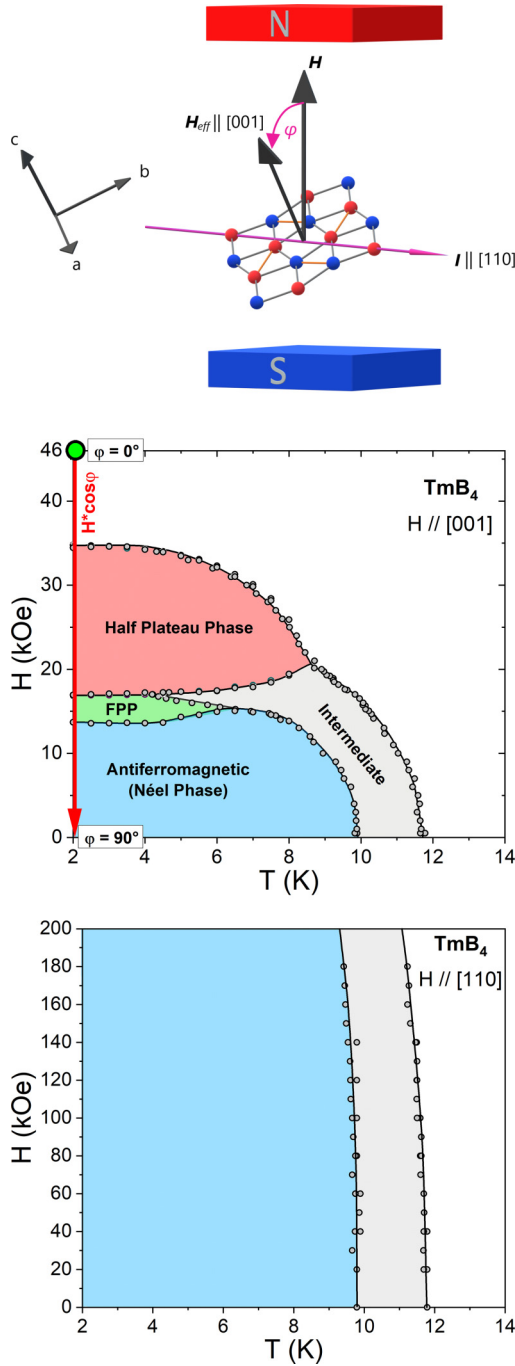


FIG. 1. Top: schematic view of angle-resolved magnetoresistance (ARMR) measurements in TmB_4 . During measurements the electrical current I flows along crystallographic direction $[110]$. The orientation of applied magnetic field H , which is always perpendicular to I , changes from direction $[001]$ via $[\bar{1}11]$ and $[\bar{1}10]$ to direction $[00\bar{1}]$, when φ is changed from 0° to 180° . Spin configuration of the antiferromagnetic ground state of the Shastry-Sutherland lattice in the a - b plane is displayed by red (spin “up”) and blue (spin “down”) spheres. Middle: phase diagram of TmB_4 for $H \parallel c$. The red arrow indicates the change of effective magnetic field, $H_{eff} = H^* \cos \varphi$, along c axis during sample rotation in field H from $\varphi = 0^\circ$ to 90° , which corresponds to the transition of sample from the saturation phase (the big green point at 2 K and $H_{eff} = 46$ kOe) to antiferromagnetic Néel phase (the end of red arrow at 2 K and $H_{eff} = 0$ kOe). Bottom: phase diagram of TmB_4 for $H \parallel [110]$.

magnetic field is a very sensitive probe of scattering processes on the magnetic order/disorder in these frustrated systems.

Here, we present a detailed study of angle-resolved magnetoresistance (ARMR) measurements that allow the construction of a complex $\Delta\rho/\rho(\varphi, H)$ mapping which provides information on scattering processes of charge carriers in various magnetic phases of TmB_4 when the applied magnetic field changes its magnitude H and orientation φ (see Fig. 1), and identify field directions where the scattering due to the magnetic structure is highest.

II. EXPERIMENT

The single crystalline TmB_4 samples were grown by an inductive, crucible-free zone melting method, with residual resistivity ratio larger than ≈ 14 , documenting their high quality. All samples were cut from one large, oriented single crystal. More information about sample preparation can be found, e.g., in [29].

Magnetoresistance $\Delta\rho/\rho(\varphi, H) = [\rho(\varphi, H) - \rho(\varphi, H=0)]/\rho(\varphi, H=0)$ measurements were performed using a standard low-frequency ac technique in a commercial PPMS unit equipped with a sample rotation option. The current $I = 5$ mA was applied along the $[110]$ direction of the Shastry-Sutherland (a - b) plane. The sample orientation to the external magnetic field H direction was changed with a step size of $\Delta\varphi = 1^\circ$ from $[001]$ via $[\bar{1}11]$ and $[\bar{1}10]$ to $[00\bar{1}]$. For this orientation there is always $H \perp I$, but the field can change its orientation from perpendicular to parallel alignment to the Shastry-Sutherland plane (for details see Fig. 1) with the rotation.

Since the magnetization of fractional magnetization plateaus depends on field history [22,26], measuring protocols were developed that reproduced the same starting points for subsequent magnetoresistance or magnetization measurements below T_N when measurements were repeated.

III. RESULTS AND DISCUSSION

Before presenting our experimental results, it is useful to elucidate the effectiveness of ARMR as a tool for anisotropy study in correlated systems. In uncorrelated compounds, magnetoresistance usually originates from the bending of the carrier trajectory in applied magnetic field. For systems with strong anisotropic behavior in magnetic field, the scattering of conduction electrons can reveal a rich intrinsic structure. The transport properties can be strongly influenced by the magnetic structure and this is reflected in very sharp changes of the MR at specific angles between applied magnetic field and crystallographic orientation of the system. However, for a successful application of ARMR high-quality single crystalline samples are inevitable, too.

A very good example is TmB_4 , where the main MR features appear for $H \parallel c$, i.e., along the easy axis of magnetic anisotropy, and correspond to magnetic phases and phase transitions between them. Results of the angular dependence of magnetoresistance $\Delta\rho/\rho(\varphi, H)$ in magnetic field up to 46 kOe and at temperatures of 13 and 2 K are shown in Fig. 2. During these measurements, as mentioned and shown above, the current I flowed in the $[110]$ direction and the magnetic

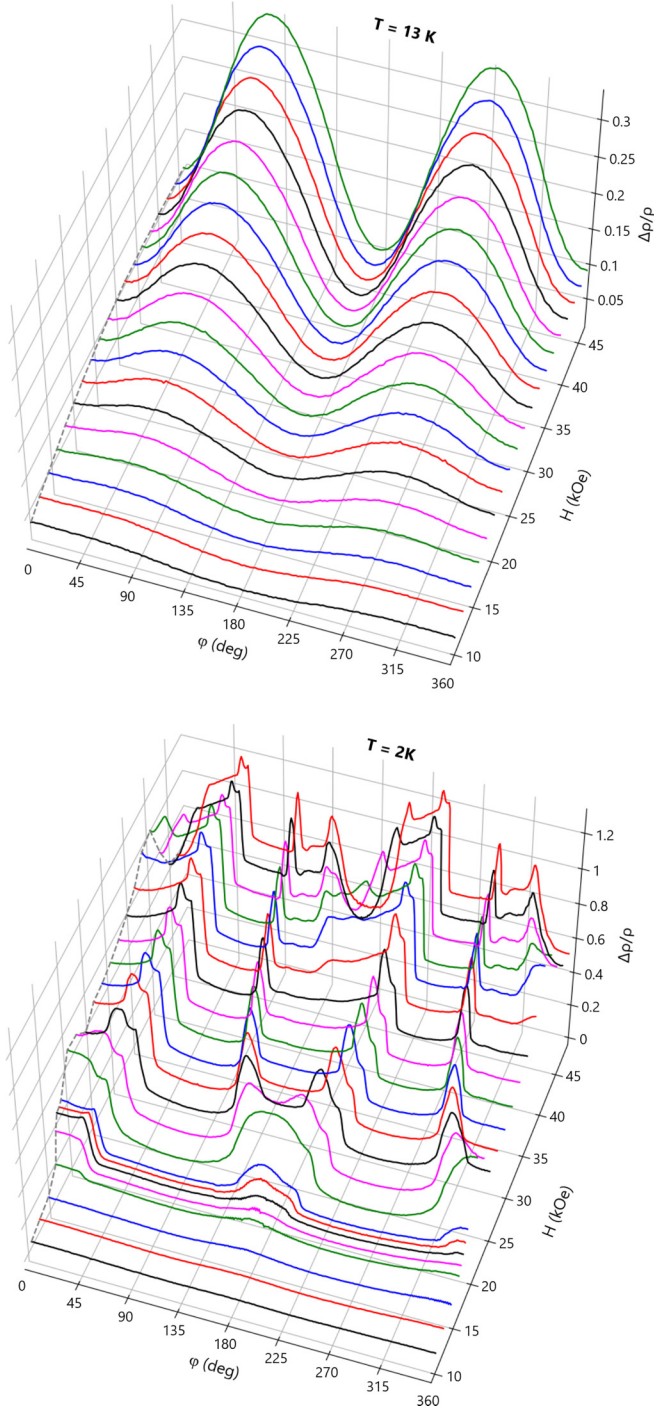


FIG. 2. Angular dependence of magnetoresistance $\Delta\rho/\rho(\varphi, H)$ of TmB_4 in various magnetic fields at 13 K (above T_N) and 2 K (below T_N). φ denotes the angle between the applied field and the c axis of sample.

field (always $H \perp I$) varied between principal crystallographic directions $[001]$, $[\bar{1}11]$, and $[\bar{1}10]$ (see Fig. 1). Thus, the MR measurements covered the full anisotropy of the tetragonal TmB_4 lattice. From Fig. 2(a) it can be seen that at 13 K (above T_N) the angular dependence of $\Delta\rho/\rho(\varphi, H)$ exhibits only basic features of the TmB_4 magnetic anisotropy: The MR reaches minima for $H \parallel c$, i.e., when H is parallel to the easy

axis of magnetization (in this case $\varphi = 0^\circ$ and/or $\varphi = 180^\circ$). Maxima are reached, as expected, when $H \perp c$, i.e., when the field is perpendicular to the easy axis. In this case the Lorentz force acting on current I forces it to flow in the direction of the c axis where the resistivity is higher than in the a - b plane ($\rho_c > \rho_{a-b}$; see, e.g., [22]).

On the other hand, at 2 K (far below T_N) the $\Delta\rho/\rho(\varphi, H)$ dependence shows distinct features of the magnetic phase transitions in TmB_4 as a function of increasing angle φ between magnetic field and the sample c axis, and as a function of applied field intensity. Moreover, the obtained $\Delta\rho/\rho(\varphi, H)$ dependence in fields higher than approximately 15 kOe are not symmetric, but exhibit clear features of hysteresis. This hysteresis (asymmetry with respect to $\varphi = 180^\circ$) might be surprising, however, it only reflects the fact that the rotation of strongly anisotropic TmB_4 in external magnetic field H manifests itself as a $H_{\text{eff}} \sim H^* \cos \varphi$ change of the field along the sample c direction (see Fig. 1 and [30]). Thus, e.g., sample or field rotation between 0° and 90° can be considered as a field lowering and the further angular change from 90° to 180° as a field increase (see Fig. 3). And, also direct $\rho(H)$ measurements between 46 kOe \rightarrow 0 kOe \rightarrow -46 kOe at 2 K show [Fig. 3(b)] that during such a field change hysteresis appears in fields where magnetic phase transitions occur.

A complete view of the angular dependence at 2 K from Fig. 2 is shown in Fig. 4, where the magnitude of $\Delta\rho/\rho(\varphi, H)$ is shown in different colors. At 13 K [Fig. 4(b)], above T_N , the highest MR is observed, as shown and explained above, for $H \perp c$ (in this case $\varphi = 90^\circ$ or 270°) and the lowest for $H \parallel c$ ($\varphi = 0^\circ$ or 180°).

Below T_N the situation changes [Fig. 4(a)]. One can see that the angular dependence of the MR is completely different, and that the largest $\Delta\rho/\rho(\varphi, H)$ anomalies appear for $H \parallel c$ and correspond to magnetic phases and phase transitions between them [similarly to the $\rho(H)$ dependence, see Fig. 3(b)]. This seemingly is related to the strong molecular field in the ordered state the origin of which is associated with quantum mechanical exchange interaction. Thus, in the ordered state the magnetic phases dominate the scattering processes of charge carriers. On the other hand, for $H \perp c$ ($\varphi = 90^\circ$ and/or 270°) no such features can be seen. This difference is related to the fact that for $H \perp c$ the field of magnetic saturation is at least ten times higher than for $H \parallel c$, and thus in a field of 46 kOe the Néel state still persists.

With increasing angle φ from 0° to 90° the MR maxima shift to higher magnetic fields. The dependence of this shift can be estimated by taking into account the above consideration that upon sample rotation the effective field along the sample c direction changes as $H_{\text{eff}} \sim H^* \cos \varphi$. Thus, as φ increases (e.g., from 0° to 90°) higher fields are needed to induce the phase transitions at which MR maxima arise (see also Fig. S3 in the Supplemental Material [31]). It can be also seen that the strongest MR features are related to the scattering of conduction electrons on the magnetic structure of the fractional plateau phase. The asymmetry of the MR, which can be seen, e.g., with respect to $\varphi = 180^\circ$ (MR to the right of $\varphi = 180^\circ$ is higher/browner than the MR on the left), can be explained by considering the fact that the rotation of this strongly anisotropic system in magnetic field H manifests itself as a cosine change of field H along the

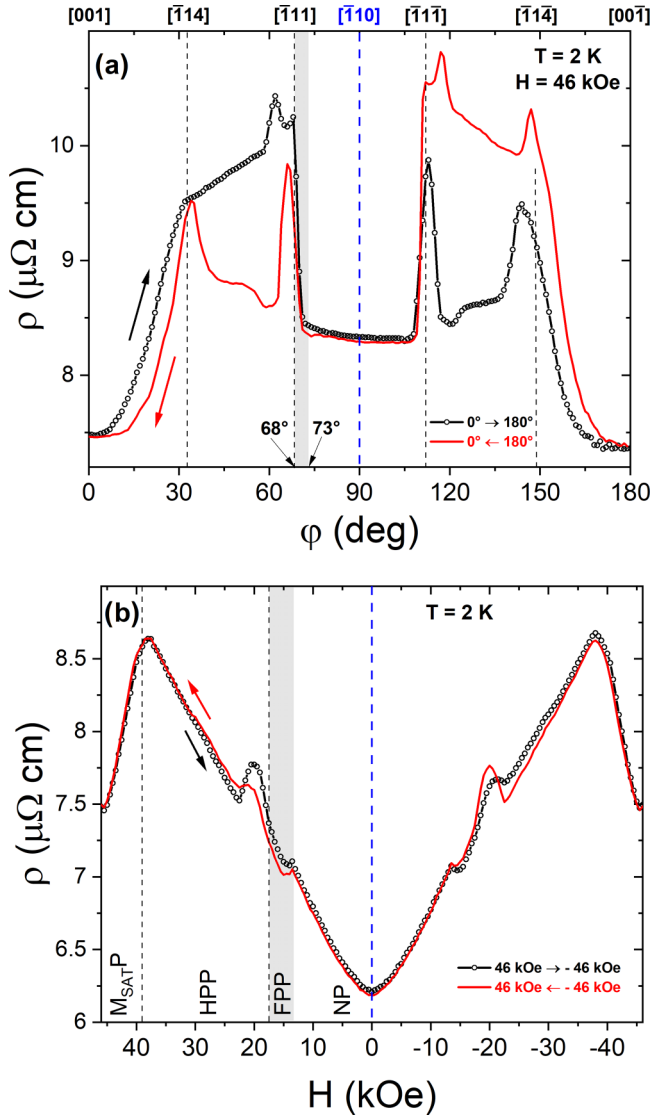


FIG. 3. (a) Angular dependence of the resistivity of TmB_4 at 2 K and in a field of 46 kOe; (b) field dependence of the resistivity $\rho(H)$ at 2 K. The starting point at 2 K and 46 kOe was reached by cooling the sample from the paramagnetic state at 20 K in field of 46 kOe. Subsequently the field was lowered to -46 kOe and then increased back to 46 kOe. Note that the hysteresis features of $\rho(H)$ appear on all magnetic phase transitions ($M_{\text{SAT}}P$: magnetization saturation phase; HPP: half plateau phase; FPP: fractional plateau phase; NP: Néel phase) that involve fractional magnetization plateaus. The shadow area on both graphs represents the fractional plateau phase.

sample c direction (mentioned already above in connection with the field dependence of resistivity in Fig. 3). The obtained precise angle-resolved magnetoresistance $\Delta\rho/\rho(\varphi, H)$ data set for current direction $I \parallel [110]$ can be displayed also in the polar presentation $\Delta\rho/\rho = f(H, \varphi)$ which is shown in Fig. S1 of [31]. One can see that at 13 K [Fig. 4(b)] the ARMР distribution is symmetric and reflects in higher fields only the strong Ising magnetic anisotropy in TmB_4 , which is present also in the paramagnetic phase above T_N . Below T_N [see Fig. 4(a)] the ARMР distribution is symmetric only in small magnetic fields, where magnetic hysteresis is not present. This suggests that ARMР is a rather sensitive experimental

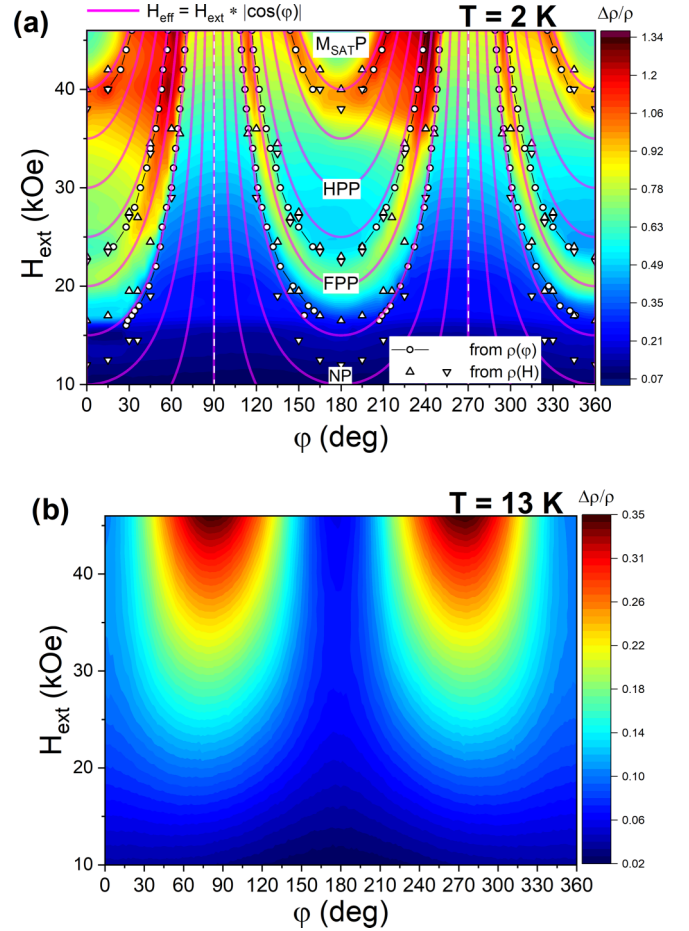


FIG. 4. Magnitude of magnetoresistance as function of angle φ and applied external magnetic field H_{ext} for current direction $I \parallel [110]$ at 2 and 13 K. Squares and circles represent phase transitions obtained from angular and field dependencies of resistivity [$\rho(\varphi)$ and $\rho(H)$], respectively. See text for a detailed description.

tool that provides additional information about the interplay between charge carriers, the various magnetic phases as a function of temperature, and the applied magnetic field and crystallographic orientations.

A similar ARMР presentation for current direction $I \parallel [001]$ is shown in Fig. S2 of [31]. In this case, however, the magnetic field ($H \perp I$) can vary only between crystallographic directions $[110]$, $[100]$, and $[1\bar{1}0]$ when φ is changed from 0° to 90° . It can be seen that for this current orientation the MR anomalies are much less pronounced and appear only in field directions, which lay between the directions mentioned above.

The obtained ARMР results are in accordance with our recent investigation of the detailed angular dependence of the rotating magnetocaloric effect (RMCE), i.e., measurements of the adiabatic change of temperature with changing angle, $\Delta T(\varphi, T, H)$ [30]. As it was shown [30], with increasing φ the heating process (due to magnetic reversal) is not monotonous, and except the expected peak at $\varphi = 90^\circ$ (when the sample was rotated from $H \parallel [001]$ to $H \perp [001]$ below T_N in H above 16 kOe) it exhibits an anomaly also around $\varphi \approx 60^\circ$. In the same study [30], angular dependent magnetization measurements at temperatures below T_N and in various magnetic fields were performed, $M(\varphi, T, H)$. It

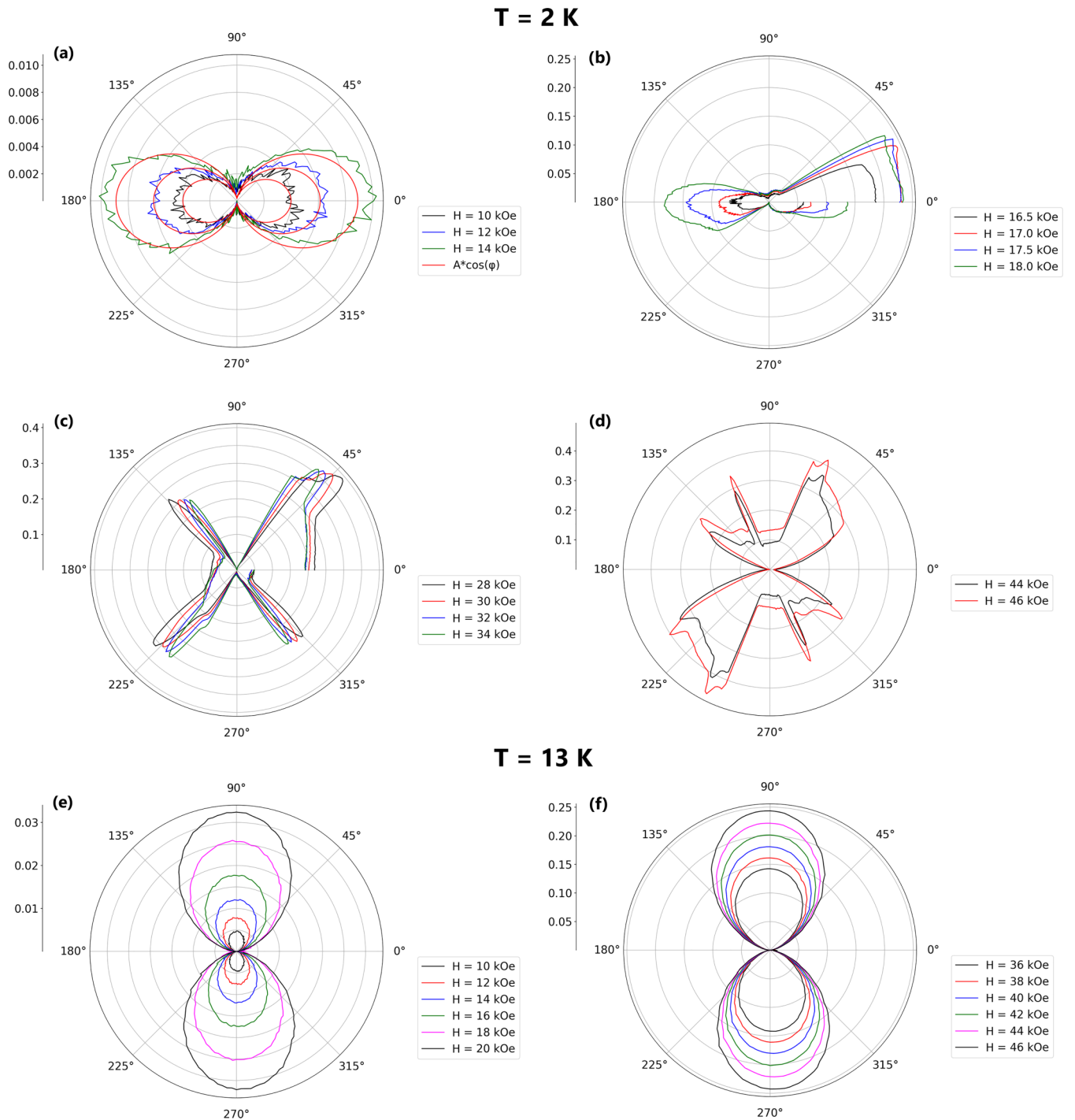


FIG. 5. Polar plots of the anisotropic magnetoresistance parameter R_{AMR} measured at $T = 2$ K (a)–(d) and $T = 13$ K (e),(f) for various fields H . The R_{AMR} shows different shapes of lobes over the full range of φ depending on value of H , i.e., on the position in magnetic phase diagram of TmB_4 : (a) in the antiferromagnetic Néel phase, (b) in the fractional plateau phase, (c) in the half plateau phase, and (d) in the saturated magnetization phase (for the location of individual phases in phase diagram see, e.g., [26]). One can see that the shape of R_{AMR} depends on the magnetic phase and exhibits various symmetries (twofold, fourfold, ...). Note moreover, that in both plateau phases also strong features of hysteresis (seen, e.g., in [26]) can be observed.

was shown that M does not anymore exhibit a sinusoidal dependence (as above T_N) when the sample is rotated from $\varphi = 0^\circ$ to $\varphi = 90^\circ$, but a rather complicated course, with an anomaly at $\varphi \approx 65^\circ$ [30]. If we assume that the rotation of an Ising system in magnetic field manifests itself as a $H_{\text{eff}} \sim H^* \cos \varphi$ field change along the c direction (see Fig. 1)

then the observed anomalies in TmB_4 below T_N and fields above 16 kOe in $\Delta T(\varphi)$ at $\varphi \approx 60^\circ$, in $M(\varphi)$ at $\varphi \approx 65^\circ$, as well as in $\rho(\varphi)$ at $\varphi \approx 68^\circ$ [see Fig. 3(a)] represent the transition to fractional plateau phase. The irreversible behavior of $\rho(\varphi)$ as well as of $\rho(H)$ (see Fig. 3) correspond very well to the fractional magnetization plateaus and to the $M(H)$

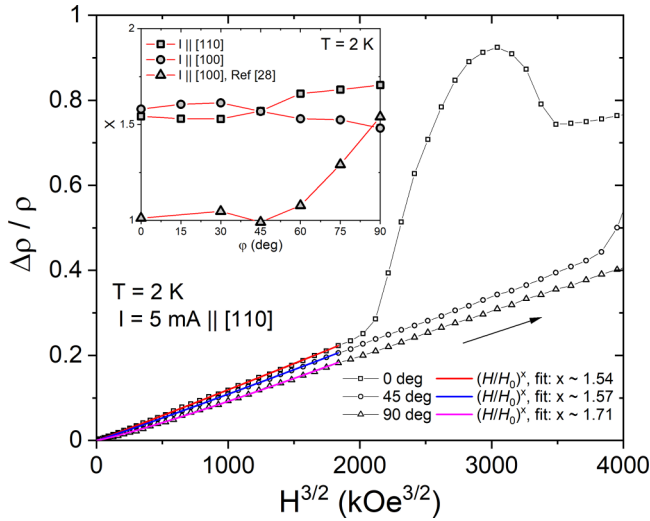


FIG. 6. The evolution of low field dependencies of magnetoresistance $\Delta\rho/\rho(\varphi, H)$ ($I \parallel [110]$) with increasing angle φ between the applied field H and the c axis, shown in $\Delta\rho/\rho$ vs $H^{3/2}$ representation. Inset shows the variation of exponent x with angle φ for two orientations of current, $I \parallel [110]$ and $I \parallel [100]$ (see [31] for the details).

hysteresis, the most distinctive feature of quantum magnet TmB_4 .

Furthermore, we investigated the strong anisotropy in TmB_4 by the calculation of anisotropic magnetoresistance parameter R_{AMR} , defined as $R_{\text{AMR}} = [R(\varphi) - R_{\text{min}}]/R_{\text{min}}$, where $R(\varphi)$ is the resistance at any φ , measured at a constant H and T , and R_{min} is the minimum resistance obtained as φ is varied. In Fig. 5, we show the variation of $R_{\text{AMR}}(\varphi)$ at $T=2$ and 13 K, respectively, for various fields. The data can be satisfactorily fitted by a $\cos(\varphi)$ dependence in low fields [for $H \leq 14$ kOe in the ordered state at 2 K, see Fig. 5(a)]. This dependence, according to [28], suggests a (quasi-)2D Fermi surface, where the MR responds to the perpendicular component of the applied field, $H^* \cos(\varphi)$, and R_{AMR} shows a twofold symmetry. In the half plateau phase [Fig. 5(c)], the twofold symmetry is changed to a fourfold one. The anisotropic MR also suggests anisotropy of the electronic effective mass [28].

To investigate the field dependence of MR in more detail, Fig. 6 shows the $\Delta\rho/\rho(\varphi, H)$ dependencies for various angles between $\varphi = 0^\circ$ and $\varphi = 90^\circ$. The analysis of the MR angle dependence shows that $\Delta\rho/\rho(\varphi, H)$ is for all angles positive and that in low magnetic fields, i.e., below ≈ 15 kOe (Néel phase), it varies as $\Delta\rho/\rho = (H/H_0)^x$, with x almost independent on φ (see inset of Fig. 6). At $\varphi = 0^\circ$ $x \approx 1.5$, and at $\varphi = 90^\circ$ $x \approx 1.7$. In the case of current along the a axis ($I \parallel [100]$), an approximately $\Delta\rho/\rho \sim H^{3/2}$ dependence over the entire angle range was observed, too (see Figs. S5 and S6 in [31]). Obtained results are not in accordance with those in [28] (see inset of Fig. 6 as well as Fig. S7 in [31]), where MR changes from a linear dependence at $\varphi = 0^\circ$ to a quadratic one at $\varphi = 90^\circ$ were observed, and where it was explained by the anisotropy of the Fermi surface topology of TmB_4 [32]. However, it is interesting that the same exponent, $x = 3/2$, was obtained for the MR dependence at $T = 2$ K and $\varphi = 90^\circ$ (see inset of Fig. 6) in the mentioned study [28].

In addition, a very similar $H^{3/2}$ behavior was observed in field dependencies of several other borides, like in simple metallic hexaboride LaB_6 [33] or in metallic high-pressure SmB_6 [34] as well as in nonmagnetic metallic dodecaboride LuB_{12} [35]. In the case of the mentioned metallic borides, the authors hypothesize that $\Delta\rho/\rho \sim H^x$ behavior with $x = 1.4$ – 1.7 and without saturation in external magnetic field $H \parallel [001]$ is due to the magnetic breakdown resulting from topological changes of the orbits, while de Haas–van Alphen measurements confirm the presence of open orbit/trajectories on the Fermi surface [34–36]. Recent studies of the crystal structure and anisotropy of the MR in LuB_{12} [35] revealed the formation of dynamic charge stripes along the $[110]$ directions, which develop due to the dynamic cooperative Jahn-Teller effect on B_{24} clusters and are associated with the modulation of the degree of hybridization of $5d$ - $2p$ band states. It is necessary to emphasize that the filamentary electron density distribution is common for all rare-earth dodecaborides but can probably develop also in other borides containing boron clusters.

The local boron environment of Tm^{3+} ions in TmB_4 can be described by B_{18} clusters, as it was shown in [32]. Then the loosely bound states of Tm^{3+} ions in TmB_4 are very similar to those in TmB_{12} with B_{24} clusters. It means that the static Jahn-Teller lattice distortion in combination with cooperative dynamic Jahn-Teller instability as well as the $5d$ - $2p$ hybridization in TmB_4 can play important role in modifying/changing the conduction band of this good metal. In addition, $5d$ - $2p$ hybridization around the Z point of the Brillouin zone was predicted from the DFT calculation leading to four-hole pockets along Γ - Z and two electron pockets around the Z point [32]. Calculated nesting of the Fermi surface around M and Z points should lead to the appearance of a charge density wave (CDW). We think that the scattering of charge carriers by the CDW may be the reason for the $3/2$ field dependence in TmB_4 , as well as in SmB_6 under pressure or LaB_6 in high fields, etc. Nesting of the Fermi surface in metallic SmB_6 just near the metal-insulator transition seems to be natural [33,34]. Such CDW scattering in rare earth dodecaborides in the temperature range 2–35 K can be the cause of the field dependence $\sim H^{1.7}$ [35].

It should be noted that similar ARMR investigations were performed very recently on dodecaborides HoLuB_{12} , HoB_{12} , and TmB_{12} [37–39]. However, those compounds with a face-centred-cubic (fcc) crystal structure have a different crystal symmetry and exhibit completely different magnetic structures. It is therefore difficult to compare results in detail.

IV. CONCLUSIONS

Precise ARMR measurements in various magnetic fields were used to obtain complete mappings of magnetotransport in the strong Ising antiferromagnet TmB_4 . The ARMR maps reveal field and crystalline directions where anomalies (maxima) of conduction electron scattering on the magnetic structure appear. It turns out that in the ordered state large scattering comes from the fractional plateau states. In fields above magnetic saturation significant MR maxima can be observed also at certain angles which correspond to specific directions in the crystal lattice. Thus, ARMR is shown to be

a sensitive tool that provides additional information about the interplay between charge carriers and various magnetic phases of the system.

ACKNOWLEDGMENTS

This work was supported by the Slovak Research and Development Agency under Contract No. APVV-17-0020,

by the Slovak Scientific Grant Agency under Contract No. VEGA 2/0032/20, as well as projects DAAD-57561069, EU ERDF (European Regional Development Fund) Grant No. VA SR ITMS2014+ 313011W856, and European Union's Horizon 2020 Research and Innovation Programme under Grant Agreement No. 824109 (European Microkelvin Platform). Liquid nitrogen for experiments was sponsored by U.S. Steel Košice, s.r.o.

- [1] A. P. Ramirez, A. Hayashi, R. J. Cava, R. Siddharthan, and B. S. Shastry, *Nature (London)* **399**, 333 (1999).
- [2] J. S. Helton, K. Matan, M. P. Shores, E. A. Nytko, B. M. Bartlett, Y. Yoshida, Y. Takano, A. Suslov, Y. Qiu, J. H. Chung, D. G. Nocera, and Y. S. Lee, *Phys. Rev. Lett.* **98**, 107204 (2007).
- [3] B. S. Shastry and B. Sutherland, *Physica B+C (Amsterdam)* **108**, 1069 (1981).
- [4] H. Kageyama, K. Yoshimura, R. Stern, N. V. Mushnikov, K. Onizuka, M. Kato, K. Kosuge, C. P. Slichter, T. Goto, and Y. Ueda, *Phys. Rev. Lett.* **82**, 3168 (1999).
- [5] K. Siemensmeyer, E. Wulf, H. J. Mikeska, K. Flachbart, S. Gabani, S. Mat'as, P. Priputen, A. Efdokimova, and N. Shitsevalova, *Phys. Rev. Lett.* **101**, 177201 (2008).
- [6] G. Will, W. Schäfer, F. Pfeifer, F. Elf, and J. Etourneau, *J. Less Common. Met.* **82**, 349 (1981).
- [7] D. Okuyama, T. Matsumura, H. Nakao, and Y. Murakami, *J. Phys. Soc. Jpn.* **74**, 2434 (2005).
- [8] D. Okuyama, T. Matsumura, T. Mouri, N. Ishikawa, K. Ohoyama, and H. Hiraka, *J. Phys. Soc. Jpn.* **77**, 044709 (2008).
- [9] J. Y. Kim, B. K. Cho, and S. H. Han, *J. Appl. Phys.* **105**, 07E116 (2009).
- [10] R. Watanuki, G. Sato, K. Suzuki, M. Ishihara, T. Yanagisawa, Y. Nemoto, and T. Goto, *J. Phys. Soc. Jpn.* **74**, 2169 (2005).
- [11] J. A. Blanco, P. J. Brown, A. Stunault, K. Katsumata, F. Iga, and S. Michimura, *Phys. Rev. B* **73**, 212411 (2006).
- [12] R. Watanuki, T. Kobayashi, R. Noguchi, and K. Suzuki, *J. Phys.: Conf. Ser.* **150**, 042229 (2009).
- [13] J. Y. Kim, N. H. Sung, B. Y. Kang, M. S. Kim, B. K. Cho, and J.-S. Rhyee, *J. Appl. Phys.* **107**, 09E111 (2010).
- [14] P. Farkašovský, H. Čenčariková, and S. Mataš, *Phys. Rev. B* **82**, 054409 (2010).
- [15] T. Verkholyak and J. Strečka, *SciPost Phys.* **12**, 056 (2022).
- [16] K. Wierschem, S. S. Sunku, T. Kong, T. Ito, P. C. Canfield, C. Panagopoulos, and P. Sengupta, *Phys. Rev. B* **92**, 214433 (2015).
- [17] S. Gabani, K. Flachbart, K. Siemensmeyer, and T. Mori, *J. Alloys Compd.* **821**, 153201 (2020).
- [18] F. Iga, A. Shigekawa, Y. Hasegawa, S. Michimura, T. Takabatake, S. Yoshii, T. Yamamoto, M. Hagiwara, and K. Kindo, *J. Magn. Magn. Mater.* **310**, e443 (2007).
- [19] S. Gabani, S. Matas, P. Priputen, K. Flachbart, K. Siemensmeyer, E. Wulf, A. Efdokimova, and N. Shitsevalova, *Acta Phys. Pol. A* **113**, 227 (2008).
- [20] S. Michimura, A. Shigekawa, F. Iga, T. Takabatake, and K. Ohoyama, *J. Phys. Soc. Jpn.* **78**, 024707 (2009).
- [21] M. C. Chang and M. F. Yang, *Phys. Rev. B* **79**, 104411 (2009).
- [22] S. S. Sunku, T. Kong, T. Ito, P. C. Canfield, B. S. Shastry, P. Sengupta, and C. Panagopoulos, *Phys. Rev. B* **93**, 174408 (2016).
- [23] S. Gabáni, I. Takáčová, M. Orendáč, G. Pristáš, E. Gažo, K. Siemensmeyer, A. Bogach, N. Sluchanko, N. Shitsevalova, J. Prokleška, V. Sechovský, and K. Flachbart, *Solid State Sci.* **105**, 106210 (2020).
- [24] J. Trinh, S. Mitra, C. Panagopoulos, T. Kong, P. C. Canfield, and A. P. Ramirez, *Phys. Rev. Lett.* **121**, 167203 (2018).
- [25] D. Lançon, V. Scagnoli, U. Staub, O. A. Petrenko, M. Ciomaga Hatnean, E. Canevet, R. Sibille, S. Francoual, J. R. L. Mardegan, K. Beauvois, G. Balakrishnan, L. J. Heyderman, Ch. Rüegg, and T. Fennell, *Phys. Rev. B* **102**, 060407(R) (2020).
- [26] Mat. Orendáč, S. Gabáni, P. Farkašovský, E. Gažo, J. Kačmarčík, M. Marcin, G. Pristáš, K. Siemensmeyer, N. Shitsevalova, and K. Flachbart, *Sci. Rep.* **11**, 6835 (2021).
- [27] L. Ye, T. Suzuki, and J. G. Checkelsky, *Phys. Rev. B* **95**, 174405 (2017).
- [28] S. Mitra, J. G. S. Kang, J. G. S. Shin, J. Q. Ng, S. S. Sunku, T. Kong, P. C. Canfield, B. S. Shastry, P. Sengupta, and C. Panagopoulos, *Phys. Rev. B* **99**, 045119 (2019).
- [29] N. Shitsevalova, Crystal Chemistry and Crystal Growth of Rare-Earth Borides, in *D. S. Inosov, Rare Earth Borides* (Jenny Stanford, Singapore, 2021), pp. 1–189.
- [30] Mat. Orendáč, S. Gabáni, E. Gažo, G. Pristáš, N. Shitsevalova, K. Siemensmeyer, and K. Flachbart, *Sci. Rep.* **8**, 10933 (2018).
- [31] See Supplemental Material at <http://link.aps.org/supplemental/10.1103/PhysRevB.107.144403> for ARMR of TmB₄ in polar coordinates for current along [110] and [100] directions at 2 K and 13 K. High field (up to 140 kOe) and low field (below 15 kOe) MR data with appropriate analyse.
- [32] J. Shin, Z. Schlesinger, and B. S. Shastry, *Phys. Rev. B* **95**, 205140 (2017).
- [33] A. J. Arko, G. Crabtree, D. Karim, F. M. Mueller, L. R. Windmiller, J. B. Ketterson, and Z. Fisk, *Phys. Rev. B* **13**, 5240 (1976).
- [34] J. C. Cooley, M. C. Aronson, A. Lacerda, Z. Fisk, P. C. Canfield, and R. P. Guertin, *Phys. Rev. B* **52**, 7322 (1995).
- [35] K. M. Krasikov, A. N. Azarevich, V. V. Glushkov, S. V. Demishev, A. L. Khoroshilov, A. V. Bogach, N. Yu. Shitsevalova, V. B. Filippov, and N. E. Sluchanko, *JETP Lett.* **112**, 413 (2020).

- [36] S. Zhang, Q. Wu, Y. Liu, and O. V. Yazyev, *Phys. Rev. B* **99**, 035142 (2019).
- [37] A. L. Khoroshilov, V. N. Krasnorussky, K. M. Krasikov, A. V. Bogach, V. V. Glushkov, S. V. Demishev, N. A. Samarin, V. V. Voronov, N. Yu. Shitsevalova, V. B. Filipov, S. Gabani, K. Flachbart, K. Siemensmeyer, S. Yu. Gavrilkin, and N. E. Sluchanko, *Phys. Rev. B* **99**, 174430 (2019).
- [38] K. Krasikov, V. Glushkov, S. Demishev, A. Khoroshilov, A. Bogach, V. Voronov, N. Shitsevalova, V. Filipov, S. Gabani, K. Flachbart, K. Siemensmeyer, and N. Sluchanko, *Phys. Rev. B* **102**, 214435 (2020).
- [39] A. Azarevich, V. Glushkov, S. Demishev, A. Bogach, V. Voronov, S. Gavrilkin, N. Shitsevalova, V. Filipov, S. Gabani, J. Kačmarčík, K. Flachbart, and N. Sluchanko, *J. Phys.: Condens. Matter* **34**, 065602 (2022).